Spin Electronics

Analysis of Skyrmion Shuffling Chamber Stochasticity for Neuromorphic Computing Applications

Zulfidin Khodzhaev[1]*, Emrah Turgut[2], and Jean Anne C. Incorvia[1]**

[1] *Department of Electrical and Computer Engineering, University of Texas at Austin, Austin, TX 78712, USA*
[2] *Department of Physics, Oklahoma State University, Stillwater, OK 74078, USA*
* *Graduate Student Member, IEEE*
** *Senior Member, IEEE*

Received 24 Mar 2023, revised 9 May 2023, accepted 17 May 2023, published 25 May 2023, current version 26 Jun 2023.

Abstract—In this study, micromagnetic simulations of a magnetic skyrmion reshuffling chamber for probabilistic computing applications are performed. The skyrmion shuffling chamber is modeled with a custom current density masking technique to capture current density variation, grain boundary variations, and anisotropy changes. The results show that the skyrmion oscillatory dynamics contribute to the system's stochasticity, allowing uncorrelated signals to be achieved with a single chamber. Our findings indicate that uncorrelated signals are generally achieved at all temperatures simulated, with the skyrmion diameter playing a role in the resulting stochasticity. Furthermore, we find that local temperature control has the benefit of not affecting the overall skyrmion diameter, while still perturbing the skyrmion trajectory. The results from varying chamber size, global temperature, and local temperature are analyzed using Pearson correlation coefficient and p-value. This research contributes to the development of tunable probabilistic computing devices and artificial synapses using magnetic skyrmions.

Index Terms—Spin electronics, magnetic devices, neuromorphic computing, probabilistic computing, skyrmion dynamics.

I. INTRODUCTION

Magnetic skyrmions are being developed, recently, for their use in computing applications. Research efforts have focused on the dynamics of skyrmions in confined geometries as well as the effects of temperature [Zázvorka 2019, Pinna 2018]. Specifically, a skyrmion reshuffling chamber for probabilistic computing has been proposed, and its efficacy is currently being explored. The major aspect of this computation is reshuffling the skyrmions to produce a constant uncorrelated signal, which is useful for addressing unwanted correlation propagation in stochastic computing [Pinna 2018], recurrent neural networks [Steil 2004], enhancing neural network performance [Rosen 2010], and efficient signal processing [Van Gerven 1994] among other applications. The chamber can also act as a tool for anomaly detection in large datasets and for adaptive filtering of data streams to improve the quality of the signal in signal processing applications. Additionally, magnetic skyrmions have demonstrated promise as artificial synapses in neuromorphic computing [Song 2020]. However, there is not yet a complete model of the skyrmion shuffling chamber that accounts for current density variation, realistic materials variations, and temperature effects together.

Here, the skyrmion reshuffling chamber is modeled in a micromagnetic simulation using a custom current density masking technique to capture current density variation. Variation due to grain boundaries and anisotropy changes is also included. We model chamber stochasticity versus temperature from 0 to 380 K, for both global temperature and local temperature change. Local temperature control could be accomplished using a localized laser, such as that used in heat-assisted magnetic recording **(HAMR)** [Kief and Victora 2018]. The resulting behavior of the skyrmion shuffler is analyzed, showing uncorrelated output signals. We find that the skyrmion oscillatory dynamics contribute to the system's stochasticity, allowing uncorrelated signals to be achieved with a single chamber. Additionally, we find that localized temperature can achieve uncorrelated signals, providing more control over the temperature response as well as reducing the need to heat the full chamber. This research aids in the development of tunable probabilistic computing devices and artificial synapses.

Corresponding author: Jean Anne C. Incorvia (e-mail: incorvia@austin.utexas.edu).
This article has supplementary downloadable material available at https://doi.org/10.1109/LMAG.2023.3280120, provided by the authors.
Digital Object Identifier 10.1109/LMAG.2023.3280120

II. MODEL

The setup of the shuffling chambers is shown in Fig. 1 for two chamber diameters: 600 nm ("small") and 2000 nm ("large") to study scaling effects. The simulation is run using MuMax3 [Vansteenkiste 2014] with the following material parameters to represent Ir/Co/Pt nonsymmetric multilayers [Moreau-Luchaire 2016]: Gilbert damping α: 0.1; saturation magnetization M_s: 9.6×10^5 A/m; anisotropy constant (0 K) 7.17×10^5 J/m^3, large chamber (110–380 K) 7.43×10^5 J/m^3, small chamber (110–380 K) 7.29×10^5 J/m^3: K_u; exchange stiffness A: 1.6×10^{-11} J/m; Dzyaloshinskii–Moriya interaction (**DMI**): 1.5×10^{-3} J/m^2.

The initial magnetization is set to be uniform out of plane ($\hat{z}$ direction). An elevated DMI in the small chamber is used to maintain skyrmion stability in the presence of increased skyrmion–skyrmion and skyrmion–edge interactions. Higher K_u values are used to counteract decrease in effective anisotropy values under high temperatures [Kwon 2020]. Damping constant $\alpha = 0.1$ was used to speed up the simulations. The discretization cell is set to 3 nm × 3 nm × 1 nm for

1949-307X © 2023 IEEE. Personal use is permitted, but republication/redistribution requires IEEE permission.
See https://www.ieee.org/publications/rights/index.html for more information.

Authorized licensed use limited to: University of Texas at Austin. Downloaded on September 05,2023 at 19:44:25 UTC from IEEE Xplore. Restrictions apply.

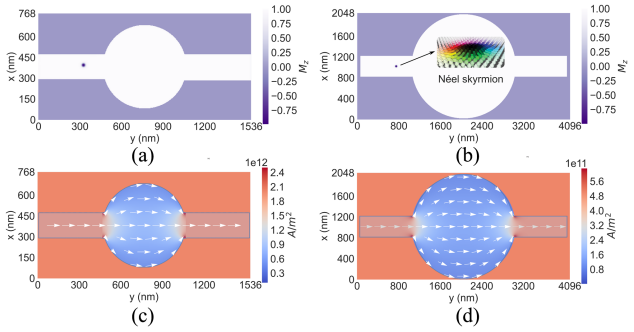

Fig. 1. Setup of the skyrmion shuffler. (a) Simulation snapshot showing initial Néel skyrmion position and magnetization M_z of the small chamber. (b) Current density of the 600 nm small chamber; current vectors depicted by white arrows. (c) Simulation snapshot showing initial Néel skyrmion position and magnetization M_z of the large chamber. The inset shows the magnified simulation snapshot of the Néel skyrmion magnetization vectors. (d) Current density of the 2000 nm large chamber.

the small chamber and 4 nm × 4 nm × 1 nm for the big chamber in the $\hat{x}$, $\hat{y}$, and $\hat{z}$ directions, respectively.

The system was modified by incorporating inhomogeneities in the form of Voronoi grain variations. Two grain sizes, 30.5 and 29.1 nm, were used for the small chamber and 98 nm for the large chamber. Grain size has been shown to affect skyrmion behavior such as skyrmion Hall angle [Legrand 2017]. The anisotropy constant for each grain was varied randomly by 0.4% and 0.3% for the large chamber and 0.3% for the small chamber.

In this letter, the term "track width" denotes the width of the rectangular input and output sections in the skyrmion shuffling chamber shown in Fig. 1. The phrases "input paths" and "output paths" correspond to the rectangular channels through which skyrmions are introduced and detected, respectively: "grain variation" for size/arrangement variation of magnetic grains and "hold period" (T_{hold}) for the time interval during which a skyrmion is held within the chamber before being released. "Stochasticity" refers to the degree of randomness in the output signal, evaluated by calculating the Pearson correlation coefficient **(PCC)** between input and output signals. Lower PCC values indicate increased stochasticity.

The simulation started by relaxing the system to its minimum energy state and then applying a current density to generate skyrmion motion. The skyrmion motion was studied for different grain sizes, currents, and geometries until stable skyrmions were generated. Then, with the initial parameters kept constant, the effect of different global and local temperatures was studied.

Fig. 1(a) and (b) shows simulation snapshots of the initial position of the Néel skyrmions introduced on the left side of the small chamber and its current density distribution, respectively. For the small chamber, skyrmions were introduced to the chamber with a 6 ns delay. For the large chamber, Fig. 1(c) and (d), skyrmions were introduced to the chamber at random, with a 10 ns delay time between each skyrmion and a 40 ns delay for 110–380 K globally applied temperatures. After shuffling inside the chamber, skyrmions entered the output path on the right. The optimal input and output track widths were determined to be 180 nm for the small and 400 nm for the large chamber, which keeps the majority of skyrmions stable and introduces stochasticity to the system.

The Laplace equation using the finite element method was used to solve for the current density along the two-dimensional shuffler

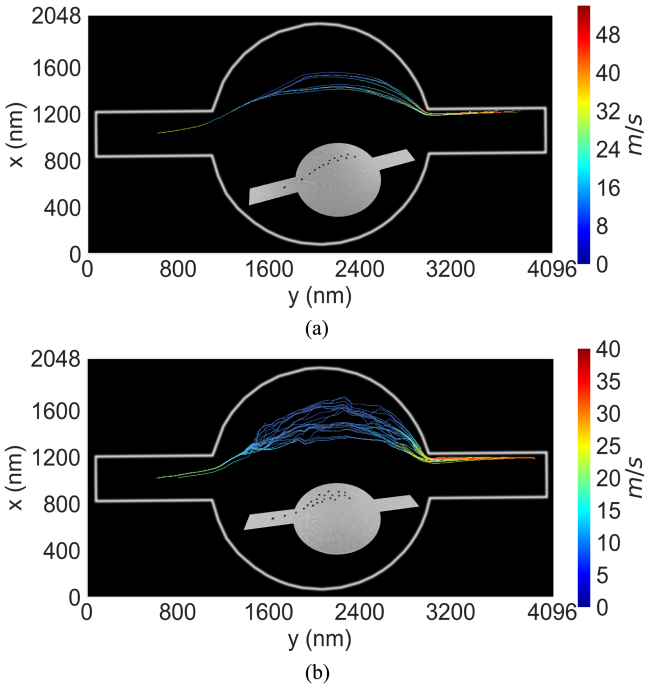

Fig. 2. Simulation results of the movement of the Néel skyrmions within a large chamber geometry and their corresponding average velocities. Multiple skyrmions are introduced to the chamber while the temperature is at 0 K, and (a) no grain variation versus (b) grain variation. Insets show simulation snapshots of the skyrmions.

structure, with the resulting current density plot shown in Fig. 1(b) and (d). The current density at the input and output is higher than the chamber's current density, and the ratio of current density inside and outside the chamber is consistent with what was observed in experimental study [Zázvorka 2019]. Masking was then used to implement the current density to each cell of the chamber in Mumax3.

III. SIMULATION RESULTS

Fig. 2 depicts the resulting skyrmion motion at 0 K, without and with random Voronoi grain variations with 98 nm grain size. The skyrmions have a projectile, predictive motion for 0 K in the absence of grain variation [Fig. 2(a)]. When grain variation is introduced into the system, stochastic interaction of the skyrmion dynamics is observed [Fig. 2(b)]. To align with experimental observations, we continue with the system that includes grain variation. The skyrmion's speed decreases as it enters the chamber and speeds up when leaving the chamber. It reaches its highest velocity at the input and output edges. These skyrmion dynamics align well with the generated current densities discussed above.

To track the trajectories of skyrmions, ImageJ [Schindelin 2012] software was employed, along with the Trackmate [Tinevez 2017, Ershov 2022] plugin. The tracking is done using images of the M_z component of the magnetization. The edges of each skyrmion are detected by measuring the y-axis mean of the M_z component of magnetization, and detection of both edges as the skyrmions move in time correlates to the skyrmion diameter, as shown in Fig. 3. This approach can detect the dynamics of the skyrmion motion and size oscillation in real time, considering a time frame of 0.3 ns between magnetizations.

Authorized licensed use limited to: University of Texas at Austin. Downloaded on September 05,2023 at 19:44:25 UTC from IEEE Xplore. Restrictions apply.

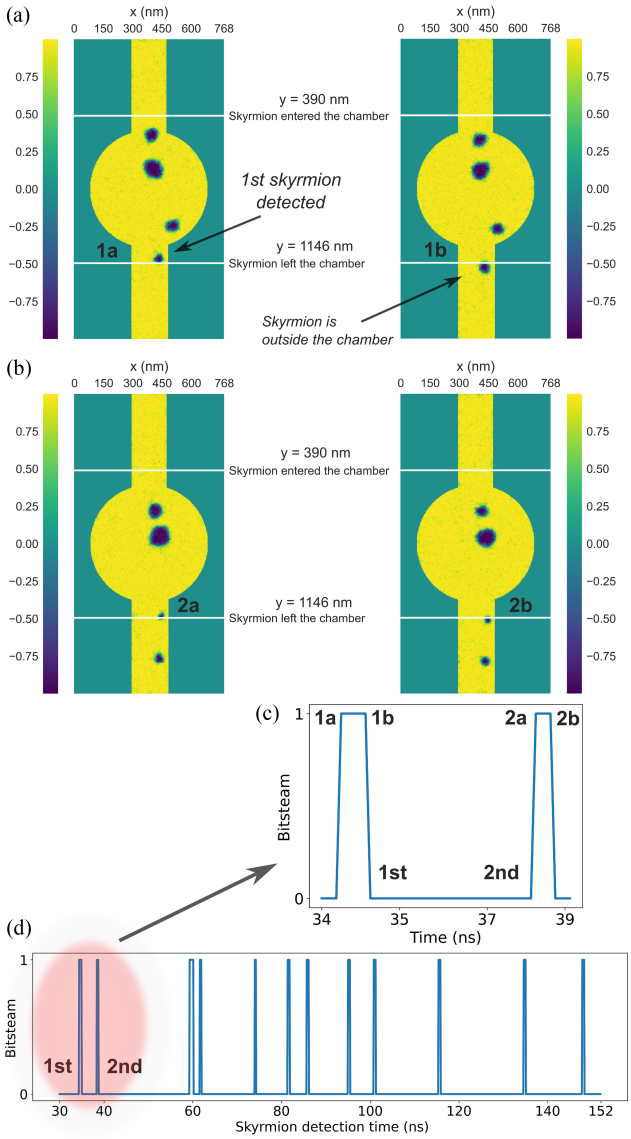

Fig. 3. Custom method used for detecting skyrmion diameter. The figure shows the detection of the edges of the first two skyrmions as they are moved to the output of the reshuffle device. The system is a small chamber measuring 600 nm and maintained at a global temperature of 203 K. (a) Detection of both edges of the first skyrmion at the output of the chamber. (b) Detection of the second skyrmion. (c) The first and second skyrmion's detected edges are connected to form a signal. (d) Complete output signals as a bitstream when the 600 nm chamber is maintained at 203 K.

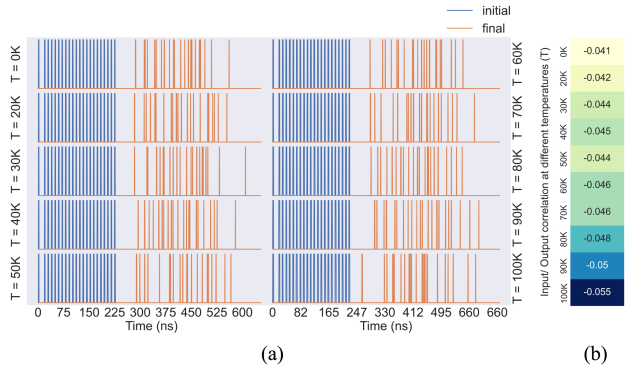

Fig. 4. Input and output signals in time for the large skyrmion shuffler, as the skyrmions are introduced on the left (blue signals) and eventually exit on the right (orange signals). (a) Results are shown for temperature 20–100 K in 10 K steps and (b) their corresponding correlation constants. Spikes indicate when the skyrmion is detected.

To observe the input/output behavior of the large skyrmion shuffler, the skyrmion position is recorded when it passes $y = 200$ nm (input) and $y = 800$ nm (output) lines. Fig. 3(a) shows the input/output for the large chamber, for temperature 20–100 K in steps of 10 K. Stochasticity is observed even at 0 K due to the grain variation. The stochastic behavior of the system was analyzed using the PCC and the p-value [Taylor 2016]. PCC is a statistical measure that quantifies the linear relationship between two variables, with values ranging from -1 (perfect negative correlation) to 1 (perfect positive correlation), and a value of 0 indicating no correlation. P-values, on the other hand, are used to assess the statistical significance of a hypothesis test, with smaller p-values (typically below 0.05) indicating stronger evidence against the null hypothesis, which assumes that there is no significant relationship between the variables being examined. However, in an experimental study on skyrmion reshufflers, 0.11 ± 0.14 correlation and $\Delta p = 0.11 \pm 0.14$ are considered highly uncorrelated and high-fidelity signals [Zázvorka 2019]. Fig. 3(b) shows, that for the range of temperatures, PCC increased from -0.04 to -0.05 as temperature increased. At the same time, the input and output's p-value trend decreased from 0.05 to 9.2×10^{-3}. As the temperature increased past 100 K, i.e., 113–383 K, the PCC values flipped from negative to positive, ranging from -0.01 to 0.14, but the p-value increased from 0.0 to 0.35. These trends in PCC and p-value can be explained by the temperature dependence of the skyrmion diameter. As temperature increases, the skyrmions start to expand, at first resulting in a modest change in correlation with skyrmion diameter/temperature. When the skyrmion diameters reach a point where they start to overlap, there is a high chance of overlap of the input/output signals. These results show, that while uncorrelated signals are generally achieved at all temperatures measured, the skyrmion diameter plays a role in the resulting stochasticity.

In this letter, as illustrated in Fig. 2, it was observed that at high current densities, skyrmions move with high velocities and can drift away from the track direction due to the Hall angle [Brearton 2021]. To address this issue, high anisotropy constant materials have been developed to be added at the edges of the racetrack, as discussed in Lai [2017]. This drifting phenomenon is evident in our simulations, particularly in the output path of the skyrmion reshuffle chamber. The skyrmion Hall angle causes skyrmions to move toward the top edge of the output path, which, in turn, increases their instability. This instability is further amplified at higher temperatures. To counteract this issue, a small strip with a higher K_u value was added to the top output path, designed to repel skyrmions from the edge and maintain their stability.

Instead of globally changing the shuffler chamber temperature, local temperature changes could be accomplished such as in HAMR using a laser. HAMR technologies use a laser beam with a width of <50 nm to write to media near 450 °C, ensuring thermal stability even for grain sizes around 5 nm diameter [Kief and Victora 2018]. The input/output shuffler dynamics for the large chamber under local temperature change are shown in Fig. 5. Two spots of 400 nm diameter, called locations a and b in Fig. 4(c), along the skyrmion trajectory are used to measure the effect of local temperate change. The center for

Authorized licensed use limited to: University of Texas at Austin. Downloaded on September 05,2023 at 19:44:25 UTC from IEEE Xplore. Restrictions apply.

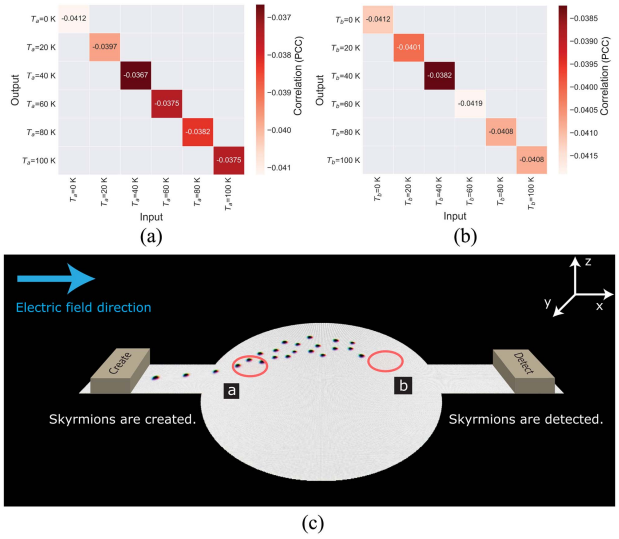

Fig. 5. (a) Heatmap showing the autocorrelation between input and output for local temperatures at the location a and $T_a = 20, 40, 60, 80, 100$ K. (b) Similarly, for location b. (c) Depiction of the location of local temperature spots (red circles) on the skyrmion shuffler for location a at $x = -400$ nm and $y = 400$ nm away from the center of the chamber (left) and location b at $x = 400$ nm and $y = 400$ nm (right).

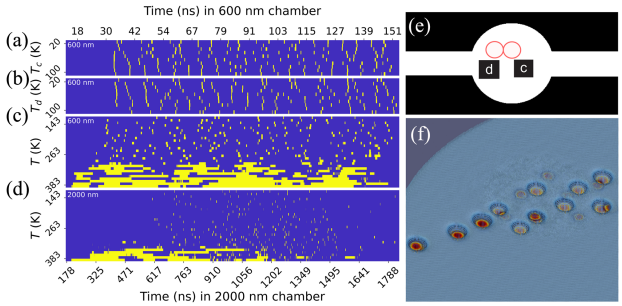

Fig. 6. Detection of a skyrmion exiting the chamber in time, recorded by each yellow data point, for different temperatures and visualization of the impact of local temperature on skyrmion dynamics. (a) For the small chamber at a local temperature location (c spot). (b) For the small chamber with location d spot. (c) For the small chamber with global temperature. (d) For the large chamber with global temperature. (e) Depiction of the location of local temperature spots on the skyrmion shuffler for location c at $x = 0$ nm and $y = 100$ nm (right) and location d at $x = -120$ nm and $y = 100$ nm (left), relative to the chamber center. (f) Two overlaid simulations, one a stable skyrmion trajectory at $T = 0$ K, the other with localized heat spot of $T = 30$ K. Color represents M_z from -1 (red) to $+1$ (blue).

location a is located at $x = -400$ nm and $y = 400$ nm, and location b at $x = 400$ nm and $y = 400$ nm, away from the center of the chamber.

Fig. 4(a) shows the autocorrelation and input/output dynamics for the large chamber and location of a spot, for 20, 40, 60, 80, and 100 K. For the local temperature located on the left, since the skyrmion trajectory is affected at the beginning of the chamber, its mean correlation (~ -0.03) is lower than the right location (~ -0.04). This might be because the local temperature effect gets amplified as skyrmions move through the chamber. The p-values ranged 0.055 ± 0.015. Fig. 4(b) shows the autocorrelation and input/output dynamics for the large chamber and location b. Uncorrelated signals can be achieved with the local temperature's position change while keeping the mean p-value the same, ranging 0.055 ± 0.016. Compared to global temperature, with local temperature, no trend in PCC versus. temperature is observed. When correlation constants are compared, it is observed that each chamber size may have its own optimum local temperature operation. However, the difference between the correlation constants is small, showing further investigation is needed. Overall, the results show that local temperature control has the benefit of not affecting the overall skyrmion diameter, while still perturbing the skyrmion trajectory.

Fig. 6 depicts the recording of each skyrmion exiting the small and large chambers over time at various temperatures, marked by yellow data points. Local temperature is applied at locations c and d in the small chamber, depicted in Fig. 5(e). Local temperatures ranging from 10 to 100 K with a temperature increment of 10 K are applied to both locations. A minor discrepancy in correlation is observed for different temperature spot locations, with the input and output signals being negatively correlated on average by 0.004 and 0.05 for locations c and d, respectively, and an average p-value of less than 0.05. The difference in the average correlation values for locations c and d is due to their distinct value distributions, with d containing only negative values, while c contains both positive and negative values, resulting in a relatively lower mean. The figure reveals the overall output pattern of signals as the temperature increases. Owing to the reduced chamber size in the small chamber, skyrmions exhibit a decreased probability of deviating from their trajectories. As the temperature increases, they necessitate a longer duration to traverse the local temperature region. This phenomenon can be attributed to the interaction between the repulsive force among skyrmions and the driving current force opposing the skyrmion's inclination to migrate from high to low temperature regions within multilayer structures [Raimondo 2022].

Fig. 5(c) and (d) illustrates the output signals of the small and large chambers, respectively, under varying global temperatures ranging from 110 to 380 K with a 10 K increment. The small chamber exhibits a correlation of 0.67% for temperatures between 110 and 350 K and 11% for temperatures between 360 and 380 K. This can be attributed to the acceleration of the expansion of the skyrmion domain beyond 360 K, which increases the likelihood of overlap with input signals. However, the edge effects of the output path limit the size of the skyrmion domain within the chamber, causing it to contract until 350 K to ensure successful passage through the output path.

Conversely, an increase in the input and output path size in the large chamber results in a decrease in the low correlation temperature range. The large chamber's input and output exhibit a negative correlation of 0.18% on average over all temperature ranges between 110 and 340 K. However, the mean correlation rises to 14.2% when the global temperature is increased up to 380 K, owing to the expansion of skyrmion domains and the resultant increase in the probability of output signals overlapping with input signals.

Global temperatures have a more substantial impact on stochasticity than local temperatures. For global temperature, input and output signals are uncorrelated in both small and large chambers. Regardless of the chamber's size, the output signals for each temperature are different.

Overall, both global and local temperature affect the system's stochasticity. This study utilized 1621 temperature data points for the small chamber and 7737 data points for the large chamber. Inclusion of additional data may further improve the p-value.

The effect of a localized heat spot on skyrmion motion is illustrated in Fig. 5(f) and the supplementary video. Two simulations are superimposed, with one simulating the skyrmion trajectory in the absence of a local temperature, and the other simulating the trajectory in the

Authorized licensed use limited to: University of Texas at Austin. Downloaded on September 05,2023 at 19:44:25 UTC from IEEE Xplore. Restrictions apply.

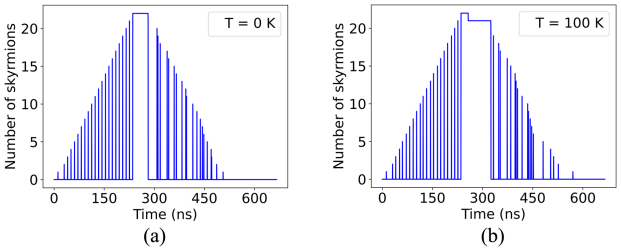

Fig. 7. Skyrmion shuffler input/output signals in time for different global temperatures in the large chamber, showing integrate and fire artificial neuron behavior using temperature. (a) Shows the time delay between integrating and firing at 0 K, while (b) shows the delay for 100 K.

presence of a local temperature of 30 K, exhibiting a randomized skyrmion position. The figure portrays the perturbation in the magnetization of each unit cell within the continuous vector field of the temperature spot, leading to a disturbance in the skyrmion trajectory over time in response to the applied temperature.

The ability to dynamically control the skyrmion shuffler chamber input/output characteristics and stochasticity using local and/or global temperature gives an additional knob for application in neuromorphic computing. The shuffler behavior maps onto the integrate and fire neuron model: integration happens as the skyrmions enter the chamber and stochastic firing happens as they exit. Fig. 7 shows the input/output behavior of the large chamber for the 0 and 100 K temperatures. It is observed that the hold period T_{hold} between when the skyrmions enter the chamber and when they start to stochastically exit increases with temperature, with $T_{\text{hold}} = (46, 48, 59, 89)$ ns for temperatures $= (70, 80, 90,$ and 100 K). This increase in the hold period can be explained by the expansion of the skyrmion domain at higher temperatures. As the temperature increases, the skyrmions have more thermal energy and occupy a larger area within the chamber. This causes the skyrmions to interact for longer periods, resulting in a longer hold period. At lower temperatures, the skyrmions are more compact and have less thermal energy. This causes their movement to be more restricted, resulting in a shorter hold period. For instance, at temperatures between 20 and 30 K, the $\Delta\ T_{\text{hold}}$ is only 0.2 ns.

It is observed that biological neurons vary their reactivity to input stimulus in the afterdepolarization process, which plays an important role in information processing and motor functions in mammalian nervous systems. Such higher-order neuronal behavior can be implemented through temperature control of the skyrmion shuffler device [Bean 2007, Llinás 1988].

IV. CONCLUSION

In summary, this letter provides a comprehensive analysis of the stochastic behavior of skyrmion shuffling chambers for use in neuromorphic computing applications, incorporating realistic materials variations and temperature effects. The results show that the skyrmion diameter affects stochasticity, and local temperature control can alter skyrmion trajectory without affecting diameter. The ability to dynamically control the skyrmion shuffling chamber's input/output characteristics and stochasticity using temperature also provides an additional knob for application in neuromorphic computing, and the shuffler behavior is shown to map onto the integrate and fire neuron model. These findings are valuable for understanding skyrmion behavior, developing tunable probabilistic computing devices, and for signal processing applications.

ACKNOWLEDGMENT

The authors acknowledge NVIDIA Corporation for the donation of the Titan Xp GPU, which was used for this research, and also the Texas Advanced Computing Center at The University of Texas at Austin for providing high-performance computing resources that contributed to the research results reported in this letter. This work was supported by the National Science Foundation under Grant 1910997.

REFERENCES

Bean B P (2007), "The action potential in mammalian central neurons," *Nat. Rev. Neurosci.*, vol. 8, pp. 451–465, doi: 10.1038/nrn2148.

Brearton R, Turnbull L A, Verezhak J A T, Balakrishnan G, Hatton P D, van der Laan G, Hesjedal T (2021), "Deriving the skyrmion Hall angle from skyrmion lattice dynamics," *Nat. Commun.*, vol. 12, 2723, doi: 10.1038/s41467-021-22857-y.

Ershov D, Phan M S, Pylvänäinen J W, Rigaud S U, Le Blanc L, Charles-Orszag A, Conway J R W, Laine R F, Roy N H, Bonazzi D, Duménil G, Jacquemet G, Tinevez J Y (2022), "TrackMate 7: Integrating state-of-the-art segmentation algorithms into tracking pipelines," *Nat. Methods*, vol. 19, pp. 829–832, doi: 10.1038/s41592-022-01507-1.

Kief M T, Victora R H (2018), "Materials for heat-assisted magnetic recording," *MRS Bull.*, vol. 43, pp. 87–92, doi: 10.1557/MRS.2018.2.

Kwon H Y, Song K M, Jeong J, Lee A-Y, Park S-Y, Kim J, Won C, Min B-C, Chang H J, Choi J W (2020), "High-density Néel-type magnetic skyrmion phase stabilized at high temperature," *NPG Asia Mater.*, vol. 12, 86, doi: 10.1038/s41427-020-00270-z.

Lai P, Zhao G P, Tang H, Ran N, Wu S Q, Xia J, Zhang X, Zhou Y (2017), "An improved racetrack structure for transporting a skyrmion," *Sci. Rep.*, vol. 7, 45330, doi: 10.1038/srep45330.

Legrand W, Maccariello D, Reyren N, Garcia K, Moutafis C, Moreau-Luchaire C, Collin S, Bouzehouane K, Cros V, Fert A (2017), "Room-temperature current-induced generation and motion of sub-100 nm skyrmions," *Nano Lett.*, vol. 17, pp. 2703–2712, doi: 10.1021/acs.nanolett.7b00649.

Llinás R R (1988), "The intrinsic electrophysiological properties of mammalian neurons: Insights into central nervous system function," *Science*, vol. 242, pp. 1654–1664, doi: 10.1126/SCIENCE.3059497.

Moreau-Luchaire C, Moutafis C, Reyren N, Sampaio J, Vaz C A F, Van Horne N, Bouzehouane K, Garcia K, Deranlot C, Warnicke P, Wohlhüter P, George J M, Weigand M, Raabe J, Cros V, Fert A (2016), "Additive interfacial chiral interaction in multilayers for stabilization of small individual skyrmions at room temperature," *Nat. Nanotechnol.*, vol. 11, pp. 444–448, doi: 10.1038/nnano.2015.313.

Pinna D, Abreu Araujo F, Kim J-V, Cros V, Querlioz D, Bessiere P, Droulez J, Grollier J (2018), "Skyrmion gas manipulation for probabilistic computing," *Phys. Rev. Appl.*, vol. 9, 64018, doi: 10.1103/PhysRevApplied.9.064018.

Raimondo E, Saugar E, Barker J, Rodrigues D, Giordano A, Carpentieri M, Jiang W, Chubykalo-Fesenko O, Tomasello R, Finocchio G (2022), "Temperature-gradient-driven magnetic skyrmion motion," *Phys. Rev. Appl.*, vol. 18, 024062, doi: 10.1103/PhysRevApplied.18.024062.

Rosen B E (2010), "Ensemble learning using decorrelated neural networks," *Funct. Foods*, vol. 8, pp. 373–384, doi: 10.1080/095400996116820.

Schindelin J, Arganda-Carreras I, Frise E, Kaynig V, Longair M, Pietzsch T, Preibisch S, Rueden C, Saalfeld S, Schmid B, Tinevez J Y, White D J, Hartenstein V, Eliceiri K, Tomancak P, Cardona A (2012), "Fiji: An open-source platform for biological-image analysis," *Nat. Methods*, vol. 9, pp. 676–682, doi: 10.1038/nmeth.2019.

Song K M, Jeong J S, Pan B, Zhang X, Xia J, Cha S, Park T E, Kim K, Finizio S, Raabe J, Chang J, Zhou Y, Zhao W, Kang W, Ju H, Woo S (2020), "Skyrmion-based artificial synapses for neuromorphic computing," *Nat. Electron.*, vol. 3, pp. 148–155, doi: 10.1038/s41928-020-0385-0.

Steil J J (2004), "Backpropagation-decorrelation: Online recurrent learning with O(N) complexity," in *Proc. IEEE Int. Conf. Neural Netw.*, vol. 2, pp. 843–848, doi: 10.1109/IJCNN.2004.1380039.

Taylor R (2016), "Interpretation of the correlation coefficient: A basic review," *J. Diagn. Med. Sonogr.*, vol. 6, pp. 35–39, doi: 10.1177/875647939000600106.

Tinevez J Y, Perry N, Schindelin J, Hoopes G M, Reynolds G D, Laplantine E, Bednarek S Y, Shorte S L, Eliceiri K W (2017), "TrackMate: An open and extensible platform for single-particle tracking," *Methods*, vol. 115, pp. 80–90, doi: 10.1016/J.YMETH.2016.09.016.

Van Gerven S, Van Compernolle D (1994), "On the use of decorrelation in scalar signal separation," in *Proc. IEEE Int. Conf. Acoust., Speech Signal Process.*, vol. 3, pp. III57–III60, doi: 10.1109/ICASSP.1994.390091.

Vansteenkiste A, Leliaert J, Dvornik M, Helsen M, Garcia-Sanchez F, Van Waeyenberge B (2014), "The design and verification of MuMax3," *AIP Adv.*, vol. 4, 107133, doi: 10.1063/1.4899186.

Zázvorka J, Jakobs F, Heinze D, Keil N, Kromin S, Jaiswal S, Litzius K, Jakob G, Virnau P, Pinna D, Everschor-Sitte K, Rózsa L, Donges A, Nowak U, Kläui M (2019), "Thermal skyrmion diffusion used in a reshuffler device," *Nat. Nanotechnol.*, vol. 14, pp. 658–661, doi: 10.1038/s41565-019-0436-8.

Authorized licensed use limited to: University of Texas at Austin. Downloaded on September 05,2023 at 19:44:25 UTC from IEEE Xplore. Restrictions apply.